Harvesting Ambient Kinetic Energy with Switched-Inductor Converters

Dongwon Kwon, *Student Member, IEEE*, Gabriel A. Rincón-Mora, *Fellow, IEEE*, and Erick O. Torres, *Member, IEEE*

***Abstract*—The potential application space for miniaturized systems like wireless microsensors is expansive, from reconnaissance mission work and remote sensors to biomedical implants and disposable consumer products. Conforming to microscale dimensions, however, constrains energy and power to such an extent that sustaining critical power-hungry functions like wireless communication is problematical. Harvesting ambient kinetic energy offers an appealing alternative, except the act of transferring energy requires power that could easily exceed what the harvester generates in the first place. This paper reviews piezoelectric and electrostatic harvester circuits, describes how to design low-power switched-inductor converters capable of producing net energy gains when supplied from piezoelectric and electrostatic transducers, and presents experimental results from prototype embodiments. In the electrostatic case shown, the controller dissipated 0.91 nJ per cycle and the switched-inductor precharger achieved 90.3% efficiency to allow the harvester to net a gain of 2.47 nJ per cycle from a capacitor that oscillated between 157 and 991 pF. The piezoelectric counterpart harnessed 1.6 to 29.6 µW from weak periodic vibrations with 0.05 – 0.16-m/s^2 accelerations and 65.3 µJ from (impact-produced) non-periodic motion.**

***Index Terms*—Harvesting/harnessing energy, vibration, piezoelectric, electrostatic, wireless microsensor, battery charger, rectifier, switched-inductor converter.**

I. Harvesting Kinetic Energy in Vibrations

Wireless microsensors can enjoy popularity in, for example, biomedical implants [1] and tire-pressure monitoring systems [2] because they offer *in-situ*, real-time, non-intrusive processing capabilities, except miniaturized platforms limit the energy onboard batteries can store, so lifetimes are short. Ambient energy is an attractive alternative because harnessing energy from light, heat, RF radiation, and motion can continuously replenish an exhaustible reservoir.

Manuscript received October 4, 2010; revised February 18, 2011; accepted April 2, 2011. This work was supported in part by the Linear Technology Corporation, Milpitas, CA, and Texas Instruments, Dallas, TX.

D. Kwon and G.A. Rincón-Mora are with the Georgia Tech Analog, Power, and Energy IC Research Lab, School of Electrical and Computer Engineering, Georgia Institute of Technology, Atlanta, GA 30332 USA (e-mail: dkwon3@gatech.edu, rincon-mora@gatech.edu).

E.O. Torres was with Georgia Tech Analog, Power, and Energy IC Research Lab, School of Electrical and Computer Engineering, Georgia Institute of Technology and is now with Texas Instruments, Dallas, TX USA (e-mail: erick.torres@gatech.edu).

Of these sources, solar light produces the highest power density, except when supplied from indoor lighting under which conditions power decreases drastically [3]. Harnessing thermal energy is viable, but microscale dimensions severely limit temperature gradients, the fundamental mechanism from which thermopiles draw power [4]–[5]. Mobile electronic devices today radiate plenty of RF energy, but still, power drops with distance to impracticable levels [6]. Harvesting kinetic energy may not compete with solar power, but in contrast to indoor lighting, thermal, and RF sources, moderate and consistent vibration power across a vast range of applications is typical [7]–[9].

Although operating conditions ultimately determine which kinetic energy-harvesting method is optimal, piezoelectric transducers are relatively mature and produce comparatively higher power than their counterparts [9]. On-chip piezoelectric devices, however, remain the subject of ongoing research [10]–[12], which is where electrostatic harvesters find an edge, because MEMS technologies can more aptly integrate variable, parallel-plate capacitors on chip [8].

Piezoelectric and electrostatic transducers harvest ambient kinetic energy by converting mechanical energy in vibrations (E_{ME} in Fig. 1) into the electrical domain (E_{EE}). More specifically, piezoelectric bimorph strips produce charge when bent and parallel-plate capacitors when their plates separate. To harness and store the generated E_{EE}, harvester circuits condition transducers and deliver a net energy gain E_{NET} to intermediate reservoirs that can supply power to electrical loads on demand. Harvesters do not supply energy to the load directly because the mechanical input is often unpredictable and therefore unreliable for sporadic loading events [13].

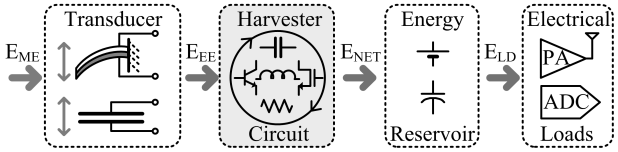

Fig. 1. Harvesting ambient kinetic energy in vibrations.

To generate E_{NET} from miniscule amounts of E_{EE}, harvesters must dissipate little. For this reason, switched-inductor circuits, which are already popular in low-power microelectronics because of their high efficiency levels, match the requirements of the harvesting function well. In addition, as this paper shows, switched-inductor converters can also condition and induce transducers to generate more E_{EE} from E_{ME} than their inductor-free and diode-based counterparts.

Accordingly, while [14] briefly introduced and described how switched-inductor circuits can harvest kinetic energy, this paper details the operation and prototype implementations of ICs designed to harvest ambient kinetic energy in vibrations with piezoelectric and electrostatic transducers. To that end, Sections II and III establish the basic harvesting theory on which illustrative piezoelectric and electrostatic switched-inductor converter examples presented rely to generate a net energy gain. Section IV then explains how these circuits dissipate (lose) power and Section V evaluates how the prototyped systems performed experimentally. The paper ends by drawing relevant conclusions in Section VI.

II. Piezoelectric Harvesters

A. Piezoelectric Transducers

When a mechanical vibration bends a piezoelectric material, the stress rearranges the internal lattice structure to shift the charge balance of the crystal [15]. Fig. 2a, for example, illustrates piezoelectricity in an ionic non-centrosymmetric crystal like quartz [16]. Here, stress shifts the centers of the positive (cations) and negative (anions) charges in opposite directions to produce a surface potential. The potential and its associated currents change continuously with variations in mechanical deformation. In essence, the material behaves as an ac current source (i_{PZT} in Fig. 2b) that charges and discharges the capacitance (C_{PZT}) across the surfaces of the material, where a leakage (R_{LEAK}) represents a slight drain [9].

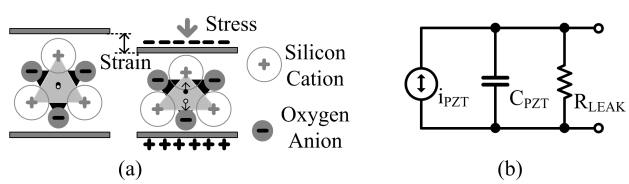

Fig. 2. (a) Ionic charges in quartz [16] and (b) equivalent circuit model.

While typical piezoelectric transducers, which are relatively mature and reliable technologies, can produce high peak voltages [17], their miniaturized counterparts cannot [10]–[12], because the amount of charge generated is proportional to strain and surface area, both of which decrease considerably with reductions in volume. Furthermore, typical environments supply mostly "weak" vibrations, energy (and voltage) from which is so low that harvesters can hardly operate.

B. Energy-Harvesting Systems

Rectifier Based: To rectify and channel the ac power that a piezoelectric transducer generates into an intermediate dc storage device, like a battery or capacitor, harvesters often employ full-wave diode-bridge rectifiers [18]–[20]. These rectifier circuits, as Fig. 3 exemplifies, steer charge to the output only when i_{PZT} charges C_{PZT} above the barrier voltage that two conducting diodes ($2V_D$) and an output capacitor C_{RECT} (V_{RECT}) produce. Since harvesting more energy amounts to channeling more of i_{PZT} into C_{RECT}, C_{RECT} is, by design, substantially larger than C_{PZT}. Accordingly, in one vibration cycle T_{VIB}, V_{RECT} remains practically unchanged and v_{PZT} clamps to the aggregate sum of $2V_D$ and V_{RECT} when i_{PZT} flows into C_{RECT} across conduction time T_{COND}.

Because leakage in piezoelectric transducers is typically negligible (i.e., R_{LEAK} is large) and C_{PZT} is a reactive component (which does not consume power), most of the energy i_{PZT} carries through the diodes reaches the output, except for the power the diodes dissipate. Rectifier efficiency η_{RECT}, the ratio of rectified output energy per cycle E_{RECT} to the input energy of the rectifier per cycle E_{EE}, therefore deteriorates with increasing diode voltage V_D:

$$\eta_{RECT} = \frac{E_{RECT}}{E_{EE}} = \frac{2\int_{T_{COND}} i_{RECT} V_{RECT} dt}{2\int_{T_{COND}} i_{PZT}\left(V_{RECT} + 2V_D\right) dt} \approx \frac{V_{RECT}}{V_{RECT} + 2V_D}. \quad (1)$$

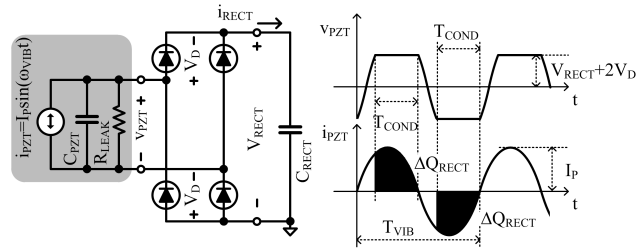

Fig. 3. Full-wave diode-bridge rectifier and relevant transducer waveforms.

Replacing the diodes with synchronous MOS switches increases η_{RECT} because MOSFETs reduce V_D from 0.5 – 0.7 V to mV's [19]–[22]. Still, a fundamental limitation with rectifiers is that v_{PZT} must exceed V_{RECT} (which represents the energy already stored in C_{RECT}) to extract energy from motion. In other words, even if V_D were zero, the rectifier stops harvesting when v_{PZT}'s open-circuit peak voltage V_P falls below V_{RECT}, which can easily happen under weak vibrations.

One way of reducing the input threshold of the rectifiers is by conditioning C_{RECT} so V_{RECT} can remain below v_{PZT}'s peak voltage [18]. This way, the system can harness some of the energy C_{PZT} receives under weak vibrations that the transducer would have otherwise transferred back into the mechanical domain. To quantify the E_{RECT} as a function of V_{RECT}, consider i_{PZT} would charge C_{PZT} from $-V_P$ to V_P with ΔQ_{PZT} (or $C_{PZT}2V_P$) without the rectifier. When the rectifier loads the transducer, because some portion of ΔQ_{PZT} is used only to charge up C_{PZT} from $-(V_{RECT}+2V_D)$ to $(V_{RECT}+2V_D)$ as shown in Fig. 3, the rectifier steers ΔQ_{RECT}:

$$\Delta Q_{RECT} = \Delta Q_{PZT} - C_{PZT}\left[2\left(V_{RECT} + 2V_D\right)\right], \quad (2)$$

into C_{RECT} (at V_{RECT}) for each half-cycle. Therefore E_{RECT} grows with V_P and become a second-order function of V_{RECT}:

$$E_{RECT} = 2\left(V_{RECT}\Delta Q_{RECT}\right) = 4V_{RECT}C_{PZT}\left[V_P - \left(V_{RECT} + 2V_D\right)\right]. \quad (3)$$

In other words, the maximum possible energy per cycle a rectifier can harness is $C_{PZT}(V_P - 2V_D)^2$, which results when V_{RECT} is $0.5(V_P - 2V_D)$. Although monitoring v_{PZT} and adjusting V_{RECT} accordingly improves performance [18], [23], sensing v_{PZT} and conditioning V_{RECT} "on the fly" can easily consume more energy than the system can harness under weak vibrations, even if V_D were zero. Here, the complexity of the system also imposes a lower bound on v_{PZT}'s V_P below which the rectifier cannot produce a net energy gain.

Switched Inductor: To circumvent the fundamental input threshold limitation rectifiers impose, the system in Fig. 4 discharges C_{PZT} into inductor L_H because C_{PZT}'s v_{PZT} energizes L_H, irrespective of how small V_P is. The switched-inductor circuit finishes the harvesting process by de-energizing L_H into battery V_{BAT}, which again, poses no threshold limit. As such, the rectifier-free, switched-inductor circuit shown can harness kinetic energy from weak vibrations.

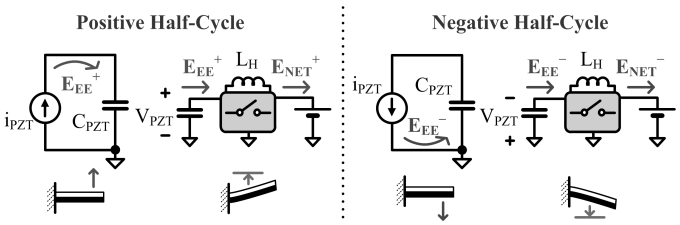

Fig. 4. Rectifier-free, switched-inductor piezoelectric energy-harvesting cycle.

The harvester in Fig. 4 first waits for vibrations to move the piezoelectric cantilever upward in the positive cycle, allowing i_{PZT} to charge C_{PZT} until v_{PZT} peaks. At the peak, the circuit quickly discharges C_{PZT} into L_H and then de-energizes L_H into V_{BAT}. Since this energy transfer only requires a few µs and the vibration cycle (T_{VIB}) is usually in ms, the position of the cantilever remains practically unchanged through this time. Afterwards, the harvester similarly waits for vibrations to charge C_{PZT} to its negative peak voltage before discharging C_{PZT} into L_H and de-energizing L_H into V_{BAT}. This inverting transfer, where the harvester charges V_{BAT} from negative v_{PZT} voltages, concludes the vibration cycle, allowing subsequent cycles to repeat the sequence as long as vibrations persist.

In the positive half cycle, C_{PZT} stores the energy produced by the transducer (E_{EE}^+) so, when the switched-inductor converter extracts it, C_{PZT} resets to 0 V. Assuming i_{PZT} is sinusoidal at $I_P\sin(\omega_{VIB}t)$ and all of it flows into C_{PZT}, v_{PZT} is

$$v_{PZT}(t) = \frac{1}{C_{PZT}}\int_0^t i_{PZT}(\tau)d\tau = \left(\frac{I_P}{\omega_{VIB}C_{PZT}}\right)\left[1-\cos(\omega_{VIB}t)\right]. \quad (4)$$

Therefore, after the positive half-cycle, C_{PZT} stores E_{EE}^+:

$$E_{EE}^+ \approx \int_0^{T/2} i_{PZT}(t)\,v_{PZT}(t)dt = \frac{2I_P^2}{\omega_{VIB}^2 C_{PZT}} = 2C_{PZT}V_P^2\,, \quad (5)$$

and the system harvests a net energy gain E_{NET}^+ that is

$$E_{NET}^+ = E_{EE}^+ - E_{LOSSES}^+\,, \quad (6)$$

where E_{LOSSES}^+ includes conduction, switching, and control-circuit losses across the circuit during the positive half-cycle.

Since the negative cycle generates an equivalent amount, the system theoretically harnesses $4C_{PZT}V_P^2$ from each period, which is four times more energy than ideal rectifiers can (at $C_{PZT}V_P^2$) under optimal operating conditions when V_D is 0V and V_{RECT} is $0.5V_P$. Fundamentally, this difference arises because the switched-inductor harvester exhausts C_{PZT} to 0 V every half cycle so C_{PZT}'s effective peak voltage increases to $2V_P$, rather than V_P, which means the electrical damping force is higher. In other words, the harvester forces the transducer to generate more E_{EE} (i.e., $0.5C_{PZT}v_{PZT}^2$) from the given E_{ME}.

Fig. 5 depicts the simplified switched-inductor power stage just described and the corresponding simulation waveforms for v_{PZT} and inductor current i_L. First, through the positive cycle, switch S_I decouples the power-stage from the transducer until v_{PZT} reaches its positive peak. The system then discharges C_{PZT} into L_H by engaging switches S_I and S_N, until i_L peaks. Since LC resonance drives this energy transfer, the system estimates L_H's energizing time by waiting for one quarter of L_H-C_{PZT}'s resonance period at $0.5\pi\sqrt{(L_HC_{PZT})}$, instead of sensing i_L's peak directly, which would otherwise require considerable power. After this, S_N opens and i_L charges the parasitic capacitance at switching node v_{SW}^+ quickly until non-inverting diode-switch D_N forward biases and depletes L_H into V_{BAT}. Note that, without a harvesting circuit, the unloaded transducer charges C_{PZT} to lower voltages $v_{PZT(UNLOADED)}$, which demonstrates the conditioning effect of the harvester.

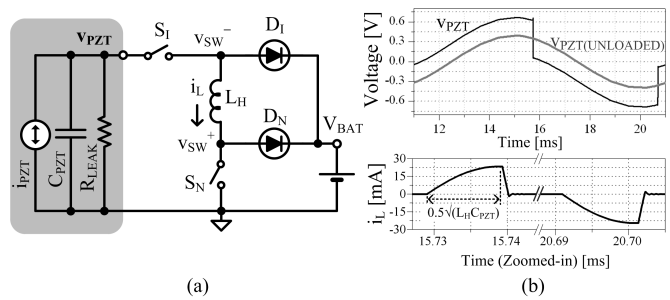

(a) (b)

Fig. 5. (a) Switched-inductor power stage and (b) simulated waveforms.

During the negative cycle, S_N decouples the circuit from the transducer until v_{PZT} reaches its negative peak. S_I and S_N then discharge C_{PZT} into L_H for one quarter of L_H-C_{PZT}'s resonance period. Afterwards, S_I opens and D_I conducts i_L into V_{BAT}.

In the end, unlike rectifier-based harvesters, the switched-inductor circuit can harness energy from small v_{PZT} voltages because L_H energizes and stores energy as soon as $|v_{PZT}|$ rises above zero. Additionally, L_H, like a current source, automatically raises the switching nodes to whatever voltage V_{BAT} defines, removing the extra dc-dc converter stage that typically bridges the voltage gap between the rectifier and V_{BAT}. In fact, dc-dc converters and other control circuits in [18] not only buffer the rectifier from the battery but also include a lossy feedback loop to optimally condition V_{RECT}. In contrast, a switched-inductor harvester can derive four times (4×) more energy than the best diode-bridge rectifier with a relatively simpler (i.e., low-power) control scheme.

C. Synchronization and Control

Fig. 6 illustrates a complete rectifier-free, switched-inductor piezoelectric harvester system. Except for the piezoelectric cantilever, L_H, and a battery, integrating all power switches and controller circuits on chip is possible. Switches S_I and S_N consist of two series NMOS transistors in an isolated p well to eliminate the undesirable conduction path the body diode would otherwise establish when using only one NMOS or PMOS switch, because the input (v_{PZT}) can swing above V_{BAT} and below ground. In the case presented, back-to-back diodes block reverse current because the p-well potential tracks the lower of the two terminal voltages present across the off-state switch. Two series PFETs would also block reverse current, but fully engaging PFETs when v_{PZT} is below ground requires

a gate-drive voltage that is well below v_{PZT}'s negative peak. In contrast, V_{BAT} is sufficiently high to engage NFETs when v_{PZT} falls below ground and v_{PZT}'s negative peak is sufficiently low to disengage them when v_{PZT} rises. Note one of the diodes always charges the p well to the most negative potential when the switch is off and the FETs short the well to the switch's terminal voltages otherwise, so the circuit always biases the well. With respect to D_N and D_I, the body terminals of M_{PDN} and M_{PDI} connect to V_{BAT} so their body diodes (*i*) block reverse (battery-discharge) current and (*ii*) clamp switching nodes v_{SW}^+ and v_{SW}^- to a diode voltage above V_{BAT}.

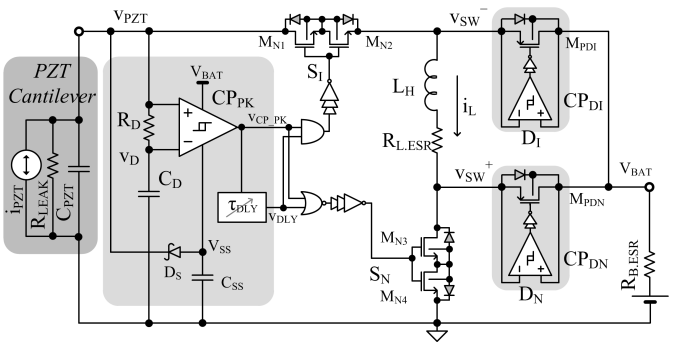

Fig. 6. Switched-inductor piezoelectric energy-harvesting system.

Peak-v_{PZT} Detector and Peak-i_L Estimator: R_D-C_D-CP_{PK} in Fig. 6 implements a peak-voltage detector that prompts the system to drain C_{PZT} into L_H when vibrations maximally charge C_{PZT}. Here, comparator CP_{PK} detects when v_{PZT} peaks by comparing v_{PZT} to its delayed counterpart v_D. To extend CP_{PK}'s input common-mode range below ground (to sense v_{PZT}'s negative peak), Schottky diode D_S and C_{SS} set negative supply voltage V_{SS}. Note that reducing power in CP_{PK} is crucial because it must detect peaks *through* the vibration period. Fortunately, the cycle is long, which means designers can trade speed for power by, for example, operating in sub-threshold. With a delay of $0.5\pi\sqrt{(L_H C_{PZT})}$, τ_{DLY} ends the C_{PZT}-to-L_H energy-transfer period. This way, with *a priori* knowledge of L_H and C_{PZT}, the system estimates (rather than sense) i_L's peak, thereby trading accuracy (and complexity) in favor of power.

Self-Synchronized Switch: As mentioned, because D_N and D_I in Fig. 5 rectify inductor currents, there is no v_{PZT} threshold below which the system cannot harness energy even if pn-junction diodes implement D_N and D_I. Still, considerable loss incurs due to their voltage drop. Replacing D_N and D_I with M_{PDN} and M_{PDI} in Fig. 6 can reduce this loss significantly.

Synchronizing M_{PDN} and M_{PDI}, however, requires precise (well-timed) control signals. If S_N and S_I's gate-control signals overlap, for example, with those of M_{PDN} and M_{PDI}, S_N-M_{PDN} and S_I-M_{PDI} might initially short-circuit V_{BAT} to ground, or to the input, which is why dead time between adjacent switches is imperative. Unfortunately, a fixed dead time in light of variable mechanical input strength, that is, an unpredictable peak inductor current, also causes additional losses [24]–[25]. With a short dead time, M_{PDN} and M_{PDI} conduct before v_{SW}^+ and v_{SW}^- reach V_{BAT}, which causes the switches to dissipate power. A long dead time, on the other hand, allows i_L to charge v_{SW}^+ and v_{SW}^- above V_{BAT}, increasing the time body diodes conduct and dissipate power. Plus, after charging the battery, disengaging M_{PDI} and M_{PDN} after v_{SW}^- and v_{SW}^+ fall below V_{BAT}, discharges the battery with reverse current.

Fundamentally, the above-mentioned losses result because M_{PDI} and M_{PDN} transition with non-zero voltages. The system in Fig. 6 reduces this loss by using comparators CP_{DI} and CP_{DN} to sense when v_{SW}^- and v_{SW}^+ reach V_{BAT}, thereby engaging M_{PDI} and M_{PDN} only when their terminals are close to 0 V. In practice, however, CP_{DI} and CP_{DN} require a finite time to respond, which on one end extends the time the lossy body-diodes conduct charging currents and on the other prompts the switches to drain the battery with reverse current.

A fast response often implies considerable quiescent current. The comparator implementation in Fig. 7 minimizes this overhead by ensuring the circuit operates only when needed: when L_H has sufficient energy to deliver to V_{BAT} and power the comparator. More explicitly, as L_H de-energizes into C_{PAR} to raise v_{SW}, some of i_L flows into mirror M_{NB}-M_{NO} to activate the comparator, which then compares the currents that M_{PB} and M_{PO}'s source-gate voltages generate. Since M_{PB} and M_{PO} match, M_{PB} drives more current and engages M_P when v_{SW} is above V_{BAT}, and vice versa otherwise. Since L_H de-energizes only twice per cycle and the required time is a small fraction of the cycle, comparator losses are low.

Because v_{SW} is initially zero, M_{PO} engages to raise v_{CP_OUT} to V_{BAT}, which ensures M_P is off. Then, L_H drives current both through M_{PB} and into C_{PAR} to power the comparator and raise v_{SW} quickly, the overdrive of which accelerates the circuit's response time. Once v_{SW} rises above V_{BAT} and M_{PB}-M_{NB}-M_{NO} lowers v_{CP_OUT}, M_P engages and v_{SW} remains above V_{BAT} by the Ohmic voltage i_L produces across M_P's series resistance. As a result, v_{SW} decreases with i_L as L_H de-energizes into V_{BAT}. When i_L reaches zero, which happens when the system depletes L_H's energy, v_{SW} drops to V_{BAT} and the comparator transitions to disengage M_P. Because i_L no longer carries sufficient current to power the comparator, the circuit shuts off automatically (i.e., synchronously).

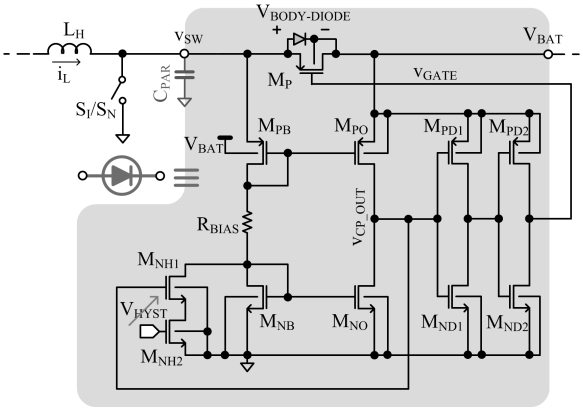

Fig. 7. Self-synchronized MOS switch M_P emulates an asynchronous diode.

During the turn-off process, the overdrive input voltage is small (because v_{SW} is near V_{BAT}) so the shut-off operation is relatively slow, which means M_P can conduct reverse current momentarily. To prevent this, the comparator raises its shut-off trip-point by leaking current away from M_{NB} through M_{NH1}

so that the circuit switches earlier, when v_{SW} is slightly above V_{BAT}. In addition to this offset for shut-off transition, M_{NH2}'s current establishes hysteresis for the turn-on transition that helps keep transient and ringing events in v_{SW} from asserting inadvertent transitions in v_{CP_OUT}.

III. Electrostatic Harvesters

A. Electrostatic Transducers

An electrostatic harvester harnesses energy from the work vibrations exert against the electrostatic force of a motion-sensitive, parallel-plate variable capacitor C_{VAR} [7]–[8]. As motion separates C_{VAR}'s plates, capacitance decreases and either C_{VAR}'s voltage v_C rises to increase its stored energy E_C or charge q_C decreases to generate current i_{HARV} as $\Delta q_C/\Delta t$.

Fabricated variable capacitors from microelectromechanical systems (MEMS) technologies in literature typically feature capacitances that range between 50 and 400 pF [26]–[30] with a maximum ΔC_{VAR} of 62 to 1570 pF [31]. In practice, these capacitors exhibit parasitic series resistances (across each parallel plate) that dissipate power and capacitances (between plates and substrate/sidewalls) that require additional charge (i.e., energy) from the system.

B. Energy-Harvesting Systems

Charge- vs Voltage-Constrained: When constraining C_{VAR}'s charge q_C (by leaving the charged C_{VAR} open-circuited) while vibrations separate C_{VAR}'s parallel plates, capacitance decreases and capacitor voltage v_C rises, augmenting the energy stored in C_{VAR} with kinetic energy from ambient vibrations. Since charge remains constant, the capacitance variation effectively amplifies C_{VAR}'s initial voltage $V_{C(INI)}$ by maximum-minimum ratio C_{MAX}/C_{MIN} to final value $V_{C(FIN)}$:

$$V_{C(FIN)} = \left(\frac{C_{MAX}}{C_{MIN}}\right) V_{C(INI)}. \quad (7)$$

Therefore, the net energy gain stored in C_{VAR} (which refers to converted mechanical energy) across a single cycle (i.e., one ΔC_{VAR} transition) is the difference between final and initial energy stored in the capacitor $E_{C(FIN)}$ and $E_{C(INI)}$:

$$E_{GAIN} = E_{C(FIN)} - E_{C(INI)} = 0.5\left(\frac{C_{MAX}}{C_{MIN}}\right)\Delta C_{VAR} V_{C(INI)}^{\ 2}. \quad (8)$$

Note $E_{C(INI)}$ is the energy required to initially charge C_{VAR}.

The challenge with keeping q_C constant is v_C can reach 100 – 300 V [32]–[33], well above the breakdown voltages of high-volume, low-cost semiconductor technologies. More expensive and specialized technologies, such as silicon-on-insulator (SOI) processes [33], can sustain these extreme voltages, but their increased costs may limit the extent to which the market will adopt them. Alternatively, keeping $V_{C(INI)}$ low enough to ensure $V_{C(FIN)}$ stays below, for example, in-package battery V_{BAT} (e.g., 2.7 – 4.2 V) reduces E_{GAIN} to

$$E_{GAIN} = 0.5\left(\frac{C_{MIN}}{C_{MAX}}\right)\Delta C_{VAR} V_{BAT}^{\ 2}. \quad (9)$$

Constraining q_C this way is compatible with low-cost, high-volume processes, but at the expense of lower E_{GAIN} (because C_{MIN}/C_{MAX} is small). What is more, transferring energy to and from C_{VAR} requires circuitry that dissipates additional power.

By holding v_C, rather than q_C, the mechanical energy that separates C_{VAR}'s plates decreases capacitance, which drives charge q_C out of C_{VAR} in the form of harvesting current i_{HARV}:

$$i_{HARV} = \frac{dq_C}{dt} = C_{VAR}\left(\frac{\partial v_C}{\partial t}\right) + V_C\left(\frac{\partial C_{VAR}}{\partial t}\right) = V_C\left(\frac{\partial C_{VAR}}{\partial t}\right). \quad (10)$$

Although constraining v_C this way is compatible with standard processes, typical implementations use an additional device (e.g., voltage source, capacitor, electret, etc.) to fix v_C [34]–[37], which contradicts the goals of integration, complicates the assembly process, and requires an energy-transferring circuit to charge the device with the harvested energy. Constraining v_C with the already-existing system battery (that is to receive charge energy) enhances integration because it does not require an additional source [38]–[41].

Switched-Inductor Harvester: A viable energy-harvesting cycle for a battery-constrained electrostatic system, as Fig. 8 illustrates, starts by precharging C_{VAR} to V_{BAT} when C_{VAR} peaks at C_{MAX}. Afterwards, connecting C_{VAR} to V_{BAT} as C_{VAR} falls to C_{MIN} steers charge (harvests) from C_{VAR} to V_{BAT}. The system then disconnects C_{VAR} and allows its voltage to drop (reset) as C_{VAR} rises again to C_{MAX}, at which point the cycle repeats. Notice that keeping C_{VAR} attached to V_{BAT} when C_{VAR} rises would draw reverse (discharge) current from V_{BAT}.

During precharge, energizing C_{VAR} at C_{MAX} to V_{BAT} represents an energy investment E_{INV} from V_{BAT} equivalent to

$$E_{INV} = 0.5 C_{MAX} V_{BAT}^{\ 2}. \quad (11)$$

Therefore, to produce a net energy gain E_{NET}, the energy harvested E_{HARV} when subsequently connecting C_{VAR} to V_{BAT} (from i_{HARV} or $V_{BAT}\Delta C_{VAR}/\Delta t$, where ΔC_{VAR} is $C_{MAX} - C_{MIN}$) must exceed E_{INV} and all other losses in the system:

$$E_{HARV} = V_{BAT}\int i_{HARV}(t)dt = \Delta C_{VAR} V_{BAT}^{\ 2} \quad (12)$$

and

$$E_{NET} = E_{HARV} - E_{INV} - E_{LOSSES} = (0.5C_{MAX} - C_{MIN})V_{BAT}^2 - E_{LOSSES}. \quad (13)$$

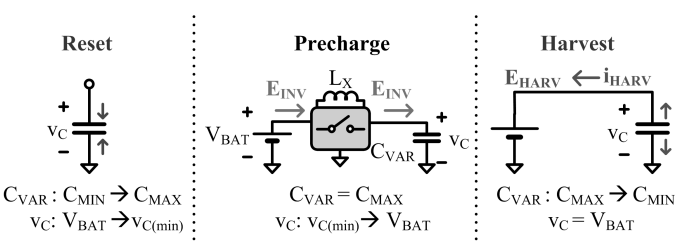

Fig. 8. Battery-constrained, switched-inductor electrostatic harvesting cycle.

When considering energy-transfer strategies to precharge C_{VAR} to V_{BAT}, the most straightforward embodiment is to connect them with a switch. With this approach, however, the switch dissipates considerable power because it conducts current while dropping a considerable voltage: the initial difference between V_{BAT} and v_C. More specifically, charging C_{VAR} at C_{MAX} from $V_{C(INI)}$ to V_{BAT} by closing a switch demands i_{BAT} from V_{BAT}, where

$$i_{BAT} = \left(\frac{V_{BAT} - V_{C(INI)}}{R_{SW}}\right)\exp\left(\frac{-t}{R_{SW}C_{MAX}}\right) \quad (14)$$

and $$v_C = V_{BAT} - i_{BAT}R_{SW}\,, \quad (15)$$
which means the switch, irrespective of R_{SW}, dissipates as much energy (E_{SW}) as C_{VAR} requires during precharge:

$$E_{SW} = \int_0^\infty i_{BAT}\left(V_{BAT} - v_C\right)dt = 0.5C_{MAX}\left(V_{BAT} - V_{C(INI)}\right)^2 = E_{INV}\,. \quad (16)$$

In other words, V_{BAT} must invest twice E_{INV} to charge C_{VAR} from $V_{C(INI)}$ to V_{BAT}, the transfer efficiency of which is 50%.

Transferring energy with an inductor (L_X), on the other hand, is virtually lossless because only a diminutive fraction of the voltage dropped appears across the interconnecting switches. In this way, the circuit in Fig. 9a transfers energy into L_X from the battery (V_{BAT}) to charge C_{VAR} to V_{BAT}. Here, V_{BAT} first energizes both L_X and C_{VAR} by closing S_E through energizing time τ_E. Then, S_E opens and S_D closes to de-energize L_X fully into C_{VAR}. S_D disengages when v_C reaches V_{BAT}, marking the end of the precharge phase. The system includes a dead time between S_E opening and S_D closing to prevent shoot-through current from discharging V_{BAT}.

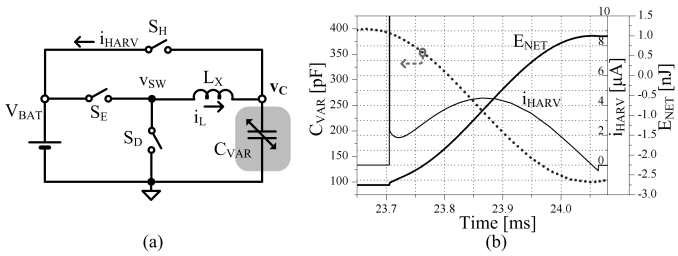

Fig. 9. (a) Switched-inductor power stage and (b) simulated waveforms.

Because this energy-transfer process only lasts a small fraction of the vibration cycle, C_{VAR} remains virtually constant (at around C_{MAX}) through the precharge phase. S_E and S_D remain off during subsequent phases of the harvesting cycle to avoid discharging C_{VAR}. The system then connects C_{VAR} to V_{BAT} with S_H to start the harvesting phase. As a result, as vibrations reduce C_{VAR} from 391 to 100 pF, for instance, as Fig. 9b demonstrates between 23.7 and 24.05 ms, i_{HARV} flows into the battery. The energy the battery accumulates in one cycle is sufficiently high to overcome its initial investment E_{INV} (at 2.75 nJ in Fig. 9b) plus the parasitic losses in the system (E_{LOSSES}) to net a gain, in this case, of 1 nJ per cycle.

C. Synchronization and Control

Fig. 10 demonstrates a circuit embodiment of the electrostatic harvester. As in the piezoelectric case, all circuit blocks, except for L_X, V_{BAT}, and transducer C_{VAR}, are on chip (where C_{VAR} can viably be on chip when integrated with a MEMS process). Similar to a buck converter, M_{PE} and M_{ND} implement L_X's energizing and de-energizing switches S_E and S_D, respectively. Harvesting switch S_H consists of back-to-back PMOS transistors M_{PHA} and M_{PHB} to ensure their parasitic body diodes do not engage during the precharge phase. All comparators only operate during their respective phases to conserve energy. Also, because vibrations are typically slow, sensing comparators $CP_{P\text{-}STRT}$ and $CP_{H\text{-}END}$, which prompt the system to start and end the precharge and harvesting phases, respectively, need not respond quickly, which means they can operate in sub-threshold (with nA's).

Reset: To precharge C_{VAR} to V_{BAT} at C_{MAX} and subsequently connect C_{VAR} to V_{BAT}, the harvester must first monitor C_{VAR}'s capacitance. Fortunately, floating C_{VAR} in the reset phase, when capacitance rises to C_{MAX}, induces v_C to fall from V_{BAT} to $V_{BAT}C_{MIN}/C_{MAX}$ (in charge-constrained fashion). Sensing, as a result, when v_C reaches its minimum voltage indicates when C_{VAR} peaks. To this end, comparator $CP_{P\text{-}STRT}$ in Fig. 10 senses when v_C begins to rise above its delayed counterpart v_D to prompt the logic to start the precharge process.

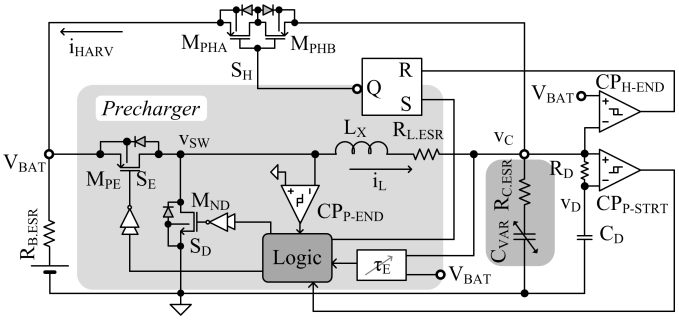

Fig. 10. Switched-inductor, voltage-constrained electrostatic harvester circuit.

Precharge: The system must determine how long (τ_E) L_X should energize to precharge C_{VAR} to V_{BAT}. Charging C_{VAR} to V_{BAT} as close as possible is critical because, with an undercharged C_{VAR}, S_H first discharges V_{BAT} to C_{VAR} before C_{VAR} can generate i_{HARV}, which represents an additional loss in the system. Overcharging C_{VAR} also incurs a loss because S_H would first discharge C_{VAR} to V_{BAT} before C_{VAR} could generate i_{HARV}. The harvester in Fig. 10 therefore uses a tuned τ_E to precharge v_C to V_{BAT} precisely. A dead time after τ_E, $CP_{P\text{-}END}$ detects when L_X depletes (i.e., i_L drops to zero) by sensing when switching node v_{SW} decreases to 0 V. $CP_{P\text{-}END}$ then triggers S_H's S-R latch to start the harvesting phase.

Instead of tuning τ_E externally, the circuit in Fig. 11 implements a feedback loop that automatically adjusts τ_E to the optimal length [41]. The loop essentially samples and compares C_{VAR}'s voltage at the end of the precharge phase ($v_{C(END)}$) to V_{BAT} and incrementally adjusts τ_E on a cycle-by-cycle basis until $v_{C(END)}$ finally reaches V_{BAT} accurately. More specifically, CP_{VC} terminates L_X's energizing time τ_E when C_{VAR} charges to intermediate voltage v_{REF}. Then, CP_{REF} compares $v_{C(END)}$ and V_{BAT} to determine whether to increment v_{REF} (and therefore τ_E) up or down until $v_{C(END)}$ nears V_{BAT}.

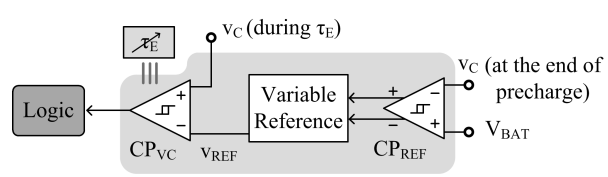

Fig. 11. Feedback loop for automatically tuning inductor energizing time τ_E.

Neglecting parasitic losses in the system, v_C should charge to $0.5V_{BAT}$ (i.e., v_{REF} is $0.5V_{BAT}$) during τ_E to end at V_{BAT} after the system exhausts L_X into C_{VAR} [40]. In practice, however, the circuit dissipates power so the system must draw more energy (than theoretical E_{INV}) from V_{BAT} to compensate for this loss, which means v_{REF} actually exceeds $0.5V_{BAT}$. Also, since precharge lasts for a diminutive fraction of the entire

cycle (e.g., about 200 ns of 33 ms), circuits in the precharge block must react quickly, which means they should operate in strong inversion. Although strong-inversion currents (i.e., power) are not small, their corresponding energy losses are because current only flows for a short while.

Harvest: In the harvesting phase, i_{HARV} flows through S_H's turn-on resistance to raise v_C slightly above V_{BAT}, keeping $CP_{H\text{-}END}$'s output from resetting S_H's S-R latch. Once C_{VAR} reaches C_{MIN} and i_{HARV} consequently falls to zero, v_C drops to V_{BAT} and $CP_{H\text{-}END}$ trips to end the harvesting phase, resetting the latch and disengaging S_H. If the system undercharges C_{VAR} in the precharge phase, $CP_{H\text{-}END}$ can trip ahead of time, possibly triggering an additional precharge event. For this reason, the harvesting phase must end when v_C falls (not rises) from above V_{BAT} to V_{BAT}, which is why the decision should rest on $C_{PH\text{-}END}$'s rising or falling edge.

IV. Energy Losses in Switched-Inductor Harvesters

The fundamental advantage of switched-inductor circuits in piezoelectric and electrostatic harvesters is efficiency, because switches conduct current when their terminal voltages are close to 0 V. While efficiencies are considerably high, conduction losses across equivalent series resistances (ESR) (in switches, inductor, and capacitors) and body diodes, switching losses from charging and discharging parasitic gate capacitances (in power switches and drivers), and bias/quiescent power (in the controller) keep efficiencies from nearing 100%. Inductor current i_L, for example, dissipates conduction power $P_{C(R)}$ across relevant ESRs. Because i_L rises and falls linearly back to zero in every cycle, these converters operate in DCM, which means losses per cycle $E_{C(R)}$ are

$$E_{C(R)} = N\left(P_{C(R)}\tau_C\right) = N\left(\frac{I_{L(PK)}}{\sqrt{3}}\right)^2 R_{EQ}\tau_C, \tag{17}$$

where N is the number of times an inductor transfers energy within one vibration cycle (e.g., two and one for the piezoelectric and electrostatic cases presented), $I_{L(PK)}$ is i_L's peak, R_{EQ} is the combined ESR of the conduction path, and τ_C is the inductor's conduction time. During the dead time (τ_{DT}) of interconnecting switches, i_L also dissipates energy $E_{C(D)}$ across conducting body diodes:

$$E_{C(BD)} = N\left(I_{L(PK)}{}^2 R_{EQ(BD)} + I_{L(PK)}V_{BD}\right)\tau_{DT}, \tag{18}$$

where $R_{EQ(BD)}$ is the combined ESR of the conduction path and V_{BD} the diode's voltage drop. (Note the self-synchronized MOSFET in Fig. 7 minimizes τ_{DT} and the loss it causes.)

During certain switching events, some transistors also dissipate I-V overlap power because they conduct current while their drain-source voltages (v_{DS}) concurrently transition several Volts. The electrostatic power-stage in Fig. 10, for example, starts the precharge phase by engaging M_{PE}, except i_L is zero when that happens so M_{PE} dissipates little power. When M_{PE} shuts off, however, i_L peaks and M_{PE} carries i_L while v_{SW} (and v_{SD}) transitions between V_{BAT} and a diode voltage (V_D) below ground, until M_{ND}'s body diode conducts i_L. When M_{PE}'s drain-gate capacitance sets overlap time τ_{OV}, M_{PE}'s average v_{SD} is $0.5(V_{BAT} + V_D)$ so $E_{SW(IV)}$ is roughly

$$E_{SW(IV)} = \left[0.5\left(V_{BAT} + V_D\right)\right] I_{L(PK)}\tau_{OV}. \tag{19}$$

M_{ND}, on the other hand, only transitions one diode voltage when engaging and i_L nears zero when disengaging, which means M_{ND} dissipates negligible overlap losses. Drivers also dissipate power to charge and discharge gate capacitances:

$$E_{SW(GD)} = \sum_{i=1}^{\#\text{ of Switches}} C_{Gi} V_{DRVi}{}^2, \tag{20}$$

where $E_{SW(GD)}$ is gate-drive energy per cycle, C_{Gi} is equivalent gate capacitance, V_{DRVi} is gate-drive voltage, and all switches (in Figs. 6 and 10) engage and disengage only once per cycle.

The controller, which generates the switching signals necessary to condition and synchronize the system to vibrations, also dissipates quiescent (bias) power. The circuits that comprise it (e.g., in Figs. 6, 10, and 11) generally fall into four categories: fast comparators, slow comparators, logic, and bias. Comparators that monitor i_L (e.g., CP_{DI}, CP_{DN}, $CP_{P\text{-}END}$, and CP_{VC} from Figs. 6 and 10), for example, must be quick because they transfer energy in sub-µs of the ms period; monitoring when C_{VAR}'s voltage peaks (e.g., CP_{REF} in Fig. 11) also occurs in sub-µs. Although these comparators require considerable strong-inversion power, they only operate for a diminutive fraction of the period, so they dissipate little energy. Comparators that monitor the transducer (e.g., CP_{PK}, $CP_{P\text{-}START}$, and $CP_{H\text{-}END}$ in Figs. 6 and 10) need not respond in µs because they monitor ms events, so they can be slow. Unfortunately, they, like bias circuits, operate through the vibration cycle, which means they can dissipate considerable energy, if not biased in sub-threshold (with nA's). Logic consumes relatively little energy because the frequency of vibrations is low (e.g., 50 – 300 Hz) and transistors are small.

Since conduction losses increase with channel resistance and switching losses with gate capacitance, smaller transistors dissipate more conduction power and less switching losses than larger ones, and vice versa. Accordingly, using minimum channel lengths and balancing transistor widths in the power stage (of Figs. 5a and 9a) are important to minimize overall losses in the system. Another design tradeoff is the number of times the inductor energizes and de-energizes in one cycle. Transferring energy multiple times, for example, increases the number of switching events (and associated switching losses) *and* decreases i_L's peak (which reduces conduction power). Also, since piezoelectric power is proportional to the square of the peak voltage, harnessing energy at the positive and negative peaks (i.e., twice per cycle) is optimal.

V. Experimental Validation

The shaker in Fig. 12 generated the periodic vibrations that validated the functionality of the circuits prototyped. The piezoelectric harvester tested used a 4.4 × 4.4 × 1.4-mm^3, 160-µH inductor with ESR of 3.4 Ω from Coilcraft and a 44 × 13 × 0.4-mm^3 piezoelectric cantilever from PiezoSystems, which with 275 nF and 10 MΩ of parasitic capacitance and resistance, resonated at about 100 Hz. The electrostatic case employed a 2 × 2 × 1-mm^3, 10-µH inductor with ESR of 1 Ω from Coilcraft and a 10.16 × 20.32 × 0.172-cm^3 variable capacitor prototype built in the laboratory (to emulate the

operation of a MEMS counterpart). At 30 Hz, the capacitor oscillated between 157 and 991 pF. A low-leakage, unity-gain op amp then monitored the voltage of the battery or capacitor that these harvesters ultimately charged.

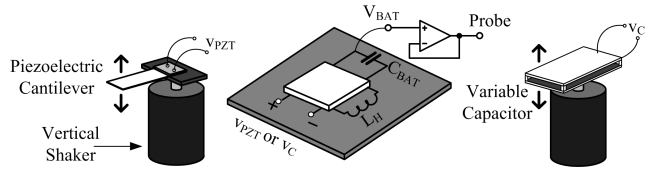

Fig. 12. Setup used to evaluate kinetic piezoelectric/electrostatic harvesters.

With this setup, the prototyped piezoelectric harvester charged 23 μF from 2.6 to 4 V in 28.5 sec. from vibrations at 100 Hz, as Fig. 13a illustrates, which represents 3.73 μW of average power, 37.3 nJ/cycle, and 106.3 μJ of total energy. In harvesting, the system increased peak piezoelectric voltages (v_{PZT}) from 0.46 (when disconnected –not shown–) to 0.65 V (when connected, as shown), which indicates the harvester conditioned the transducer to induce it to generate more power. Similarly, Fig. 13b shows the operation of the prototyped electrostatic harvester charging 1 μF from 2.7 to 4.2 V in 68.8 sec. from vibrations at 30 Hz, which equates to 75.2 nW of average power, 1.930 and 3.885 nJ/cycle at 2.7 and 4.2 V, and 5.12 μJ of total energy.

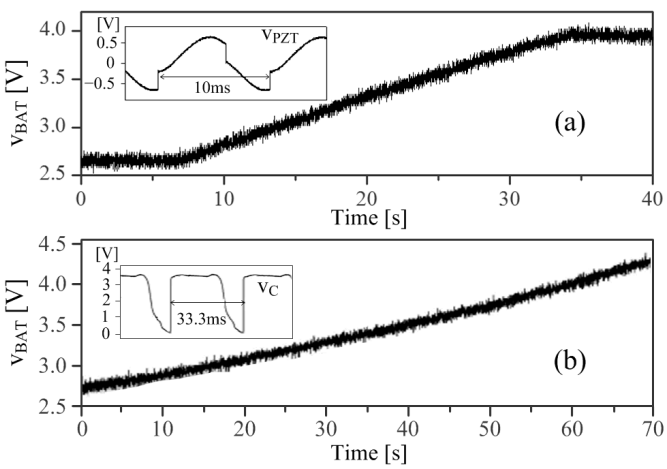

Fig. 13. Experimental (a) piezoelectric and (b) electrostatic charging profiles.

When charging a 3.5-V battery, the prototyped electrostatic harvester drew (on average) up to 505 nA from C_{VAR} [40]–[41]. The 10.1 nJ/cycle gained was sufficient to overcome V_{BAT}'s initial 6.72 nJ/cycle precharge investment in C_{VAR}. Since 991 pF requires 6.07 nJ to precharge to 3.5 V, the switched-inductor precharger's efficiency was 90.3%. The prototype kept lost quiescent energy E_Q in the controller low at 0.91 nJ/cycle by operating fast, power-hungry blocks only on-demand and their slower counterparts in sub-threshold with nA's. After subtracting the initial investment and all other losses in the system (from Table I), the net energy gain per cycle was 2.47 nJ, which is equivalent to 74.1 nW at 30 Hz.

TABLE I. MEASURED ENERGY PER CYCLE IN THE ELECTROSTATIC HARVESTER PROTOTYPE.

Phase	Component	I_Q	t_{ON}	E_Q
Reset	$CP_{P\text{-}START}$	2.0 nA	13.3 ms	0.095 nJ
	CP_{VC}	28.0 μA	230 ns	0.023 nJ
Precharge	$CP_{P\text{-}END}$	22.4 μA	253 ns	0.020 nJ
	Local μA-Bias	12.4 μA	500 ns	0.022 nJ
Harvest	$CP_{H\text{-}END}$	3.0 nA	20 ms	0.21 nJ
Optimal τ_E-Tuning	CP_{REF}	42.3 μA	489 ns	0.072 nJ
	Variable Reference	34.0 μA	489 ns	0.058 nJ
Global	nA-Bias Generator	3.5 nA	33.3 ms (T_{VIB})	0.41 nJ

The prototyped piezoelectric harvester drew 1.6 to 29.6 μW [42]–[43] from periodic vibrations with accelerations at the base of the cantilever that ranged from 0.05 to 0.16 m/s^2 – note typical HVAC vents in the office exhibit accelerations that exceed 0.2 m/s^2 [8]. Efficiency remained below 50%, as Fig. 14a shows, because conduction losses P_C dominate over their switching and quiescent counterparts P_{SW} and P_Q. Improving efficiency here is possible by decreasing resistances (i.e., power losses) in the conduction path, that is, by balancing losses. In other words, enlarging the switches and using a physically larger inductor, which has lower equivalent series resistance (ESR), increases efficiency, as the simulated results in Fig. 14b demonstrate (with switches that are 10× larger and a 0.84-Ω 160-μH inductor that is 5 × 5 × 3 mm^3). The tradeoff, of course, is space (i.e., cost) because both die size and board space increase. Nevertheless, with these values, P_C decreases more than gate-drive losses (P_{SW}) increase, and efficiency, as a result, reaches 75%. The design, however, is now optimum for a higher power range, which means efficiency drops below 50% at lower power levels, when P_{SW} and P_Q dominate. Plus, increasing the power range beyond the balanced region again induces P_C to dominate and efficiency to suffer.

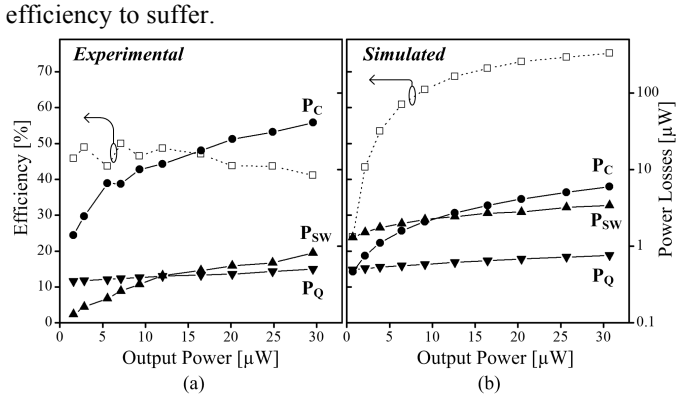

Fig. 14. Efficiency and losses in the piezoelectric harvester with physically (a) smaller (experimental) and (b) larger (simulated) switches and inductor.

In practice, real-life vibrations are often non-periodic, such as in the case of an object crashing. In this regard, Fig. 15 demonstrates that the piezoelectric system charged 23 μF from 3.05 to 3.43 V and then to 3.87 V with 65.3 μJ from vibrations generated by striking the table on which the setup of Fig. 12 rested. Generally, this system can harness energy from non-periodic vibrations as long as (*i*) it can detect when v_{PZT} peaks (to draw energy before the transducer converts it back into the

mechanical domain) and (*ii*) the energy-transfer process is shorter than the vibration period.

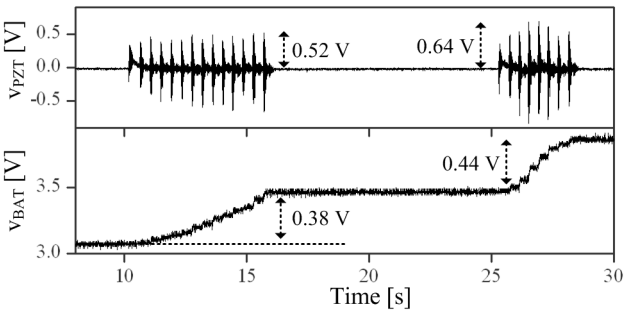

Fig. 15. Experimental (piezo-) charging profile from non-periodic vibrations.

VI. Conclusion

Since energy per cycle is low in miniaturized systems and synchronizing a circuit to vibrations and transferring energy dissipate power, the fundamental challenge in harvesting kinetic energy is producing a net energy gain, in other words, reducing losses. This paper presents a tutorial on how switched-inductor converters can not only diminish losses in energy-harvesting systems but also condition the transducer's voltage to expand the harvestable vibration range and therefore induce the transducer to draw more energy from vibrations. Inductors, however, are bulky and difficult to integrate, which is why using only one is so important. Still, tiny transducers generate little power and may therefore lose a considerable portion to conduction and switching losses, reducing efficiencies to 40%. When optimally designing the switches, inductor, and number of switching events for the power level targeted, efficiency performance can potentially surpass 90%, even when transferring only 6.7 nJ per cycle. To reduce quiescent losses to less than 1 nJ per cycle, the slow portions of the controller should operate in sub-threshold with ultra-low currents and fast blocks, which require more current, operate for a diminutive fraction of the vibration period. After all, continuously generating output power, even if only a few nW's or µW's, can charge a battery so, when a sensor needs energy, which typically does not happen often, the battery can readily supply it. The idea is to supplement the system with enough energy over time to extend its operational life and avoid having to replace an exhaustible battery.

References

[1] D.A. La Van, *et al*., "Small-scale systems for in vivo drug delivery," *Nature Biotechnology*, vol. 21, no. 10, pp. 1184–1191, Oct. 2003.

[2] M. Flatscher, *et al*., "A bulk acoustic wave (BAW) based transceiver for an in-tire-pressure monitoring sensor node," *IEEE J. Solid-State Circuits*, vol. 45, no. 1, pp. 167–177, Jan. 2010.

[3] N.J. Guilar, *et al*., "Integrated solar energy harvesting and storage," *IEEE Trans. VLSI Syst.*, vol. 17, no. 5, pp. 627–637, May 2009.

[4] H. Lhermet, *et al*., "Efficient power management circuit: from thermal energy harvesting to above-IC microbattery energy storage," *IEEE J. Solid- State Circuits*, vol. 43, no. 1, pp. 246-255, Jan. 2008.

[5] E.J. Carlson, *et al*., "A 20 mV input boost converter with efficient digital control for thermoelectric energy harvesting," *IEEE J. Solid-State Circuits*, vol. 45, no. 4, pp. 741–750, Apr. 2010.

[6] T. Le, *et al*., "Efficient far-field radio frequency energy harvesting for passively powered sensor networks," *IEEE J. Solid-State Circuits*, vol. 43, no. 5, pp. 1287–1302, May 2008.

[7] P.D. Mitcheson, *et al*., "Energy harvesting from human and machine motion for wireless electronic devices," *Proceedings of the IEEE*, vol. 96, no. 9, pp. 1457-1486, Sept. 2008.

[8] S. Roundy, *et al*., *Energy Scavenging for Wireless Sensor Networks with Special Focus on Vibrations*, 1st ed., Boston, MA: Kluwer Academic Publishers, 2004.

[9] S. Priya and D.J. Inman, *Energy Harvesting Technologies*, New York, NY: Springer Science+Business Media, LLC 2009.

[10] W.J. Choi, *et al*., "Energy harvesting MEMS device based on thin film piezoelectric cantilevers," *J. Electroceram.*, vol. 17, pp. 543–548, 2006.

[11] M. Renaud, *et al*., "Fabrication, modelling and characterization of MEMS piezoelectric vibration harvesters," *Sensors and Actuators A (Physical)*, vol. 145-146, pp. 380-386, July-Aug. 2008.

[12] B.-S. Lee, *et al*., "Comparison of the piezoelectric MEMS generators with interdigital electrodes and laminated electrodes," in *Proceedings of the SPIE-The International Society for Optical Engineering*, March 2008, pp. 69331B-1–69331B-8.

[13] D. Kwon and G.A. Rincón-Mora, "A rectifier-free piezoelectric energy harvester circuit," *Proc. IEEE International Symposium on Circuits and Systems (ISCAS)*, pp. 1085-1088, May 2009.

[14] D. Kwon, *et al*., "Harvesting kinetic energy with switched-inductor dc-dc converters," *Proc. IEEE International Symposium on Circuits and Systems (ISCAS)*, pp. 281–284, May 2010.

[15] S.D. Senturia, *Microsystem Design,* 1st ed., Boston, MA: Kluwer Academic Publishers, 2001.

[16] M.J. Madou, *Fundamentals of Microfabrication*, 1st ed., Boca Raton, FL: CRC Press, 1998.

[17] L. Steinke, *et al*., "Piezoelectric igniter for gaseous fuels or the like," U.S. Patent 3 457 461, July 22, 1969.

[18] G.K. Ottman, *et al*., "Adaptive piezoelectric energy harvesting circuit for wireless remote power supply," *IEEE Trans. Power Electronics*, vol. 17, no. 5, pp. 669–676, Sept. 2002.

[19] T. Le, *et al*., "Piezoelectric micro-power generation interface circuits," *IEEE J. Solid-State Circuits*, vol. 41, no. 6, pp. 1411-1420, June 2006.

[20] N.J. Guilar, *et al*., "A full-wave rectifier with integrated peak selection for multiple electrode piezoelectric energy harvesters," *IEEE J. Solid-State Circuits*, vol. 44, no.1, pp. 240-246, Jan. 2009.

[21] Y.H. Lam, *et al*., "Integrated low-loss CMOS active rectifier for wirelessly powered devices," *IEEE Trans. Circuits Syst. II*, vol. 53, no. 12, pp. 1378–1382, Dec. 2006.

[22] S. Guo and H. Lee, "An efficiency-enhanced CMOS rectifier with unbalanced-biased comparators for transcutaneous-powered high-current implants," *IEEE. J. Solid-State Circuits*, vol. 44, no. 6, pp. 1796–1804, June 2009.

[23] C. Lu, *et al*., "A batteryless vibration-based energy harvesting system for ultra low power ubiquitous applications," *Proc. IEEE International Symposium on Circuits and Systems (ISCAS)*, pp. 1349-1352, May 2007.

[24] T.Y. Man, *et al*., "A 0.9-V input discontinuous-conduction-mode boost converter with CMOS-control rectifier," *IEEE J. Solid-State Circuits*, vol. 43, no. 9, pp. 2036–2046, Sept. 2008.

[25] H. Lee and S.-R. Ryu, "An efficiency-enhanced DCM buck regulator with improved switching timing of power transistors," *IEEE Trans. on Circuits and Systems II*, vol. 57, no. 3, pp. 238-242, March 2010.

[26] S. Meninger, *et al*., "Vibration-to-electric energy conversion," *IEEE Trans. on Very Large Scale Integration (VLSI) Systems*, vol. 9, no. 1, pp. 64-76, Feb. 2001.

[27] S.P. Beeby, *et al*., "Energy harvesting vibration sources for microsystems applications," *Measurement Science and Technology*, vol. 17, no. 12, pp. R175-195, Dec. 2006.

[28] P.D. Mitcheson, *et al*., "MEMS electrostatic micropower generator for low frequency operation," *Sensors and Actuators A: Physical*, vol. 115, no. 2-3, pp. 523-529, Sept. 2004.

[29] G. Despesse, *et al*., "Design and fabrication of a new system for vibration energy harvesting," *Proc. PhD. Research in Microelectronics and Electronics*, vol. 1, pp. 225-228, July 2005.

[30] M. Miyazaki, *et al*., "Electric-energy generation using variable-capacitive resonator for power-free LSI: efficiency analysis and fundamental experiment," *Proc. International Symposium on Low Power Design*, pp. 193-198, Aug. 2003.

[31] Y. Chiu and V.F.G. Tseng, "A capacitive vibration-to-electricity energy converter with integrated mechanical switches," *J. of Micromechanics and Microengineering*, vol. 18, no. 10, pp. 1-8, Oct. 2008.

[32] B.H. Stark, *et al*., "Converter circuit design, semiconductor device selection and analysis of parasitics for micropower electrostatic

generators," *IEEE Trans. on Power Electronics*, vol. 21, no. 1, pp. 27-37, Jan. 2006.

[33] B.H. Stark and T.C. Green "Comparison of SOI power device structures in power converters for high-voltage, low-charge electrostatic microgenerators," *IEEE Trans. on Electron Devices*, vol. 52, no. 7, pp. 1640-1648, July 2005.

[34] R. Tashiro, *et al*., "Development of an electrostatic generator that harnesses the motion of a living body," *JSME International J, Series C: Mechanical Systems, Machine Elements and Manufacturing*, vol .43, no. 4, pp. 916-922, Dec. 2000.

[35] B.C. Yen and J.H. Lang, "A variable-capacitance vibration-to-electric energy harvester," *IEEE Trans. on Circuits and Systems I*, vol. 53, no. 2, pp. 288-295, Feb. 2006.

[36] F. Peano and T. Tambosso, "Design and optimization of a MEMS electret-based capacitive energy scavenger," *IEEE J. of Microelectromechanical Systems (MEMS)*, vol. 14, no. 3, pp. 429-435, June 2005.

[37] W. Ma, *et al*., "An integrated floating-electrode electric microgenerator," *IEEE J. of Microelectromechanical Systems (MEMS)*, vol. 16, no. 1, pp. 29-37, Feb. 2007.

[38] E.O. Torres and G.A. Rincón-Mora, "Electrostatic energy-harvesting and battery-charging CMOS system prototype," *IEEE Trans. on Circuits and Systems I*, vol. 56, no. 9, pp. 1938-1948, Sept. 2009.

[39] E.O. Torres and G.A. Rincón-Mora, "Energy budget and high-gain strategies for voltage-constrained electrostatic harvesters," *Proc. IEEE International Symposium on Circuits and Systems (ISCAS)*, pp. 1101-1104, May 2009.

[40] E.O. Torres and G.A. Rincón-Mora, "A 0.7-µm BiCMOS electrostatic energy-harvesting system IC," *IEEE J. of Solid-State Circuits*, vol. 45, no. 2, pp. 483-496, Feb. 2010.

[41] E.O. Torres and G.A. Rincón-Mora, "Self-tuning electrostatic energy-harvester IC," *IEEE Trans. on Circuits and Systems II*, vol. 57, no. 10, pp. 808-812, Oct. 2010.

[42] D. Kwon and G.A. Rincón-Mora, "A single-inductor AC-DC piezoelectric energy-harvester/battery-charger IC converting ±(0.35 to 1.2V) to (2.7 to 4.5V)," in *IEEE Int. Solid-State Circuits Conf. (ISSCC) Dig. Tech. Papers*, Feb. 2010, vol. 53, pp. 494-495.

[43] D. Kwon and G.A. Rincón-Mora, "A 2-µm BiCMOS Rectifier-free AC-DC Piezoelectric Energy Harvester-Charger IC," *IEEE Trans. on Biomedical Circuits and Systems*, vol. 4, no. 6, pp. 400-409, Dec. 2010.

Dongwon Kwon (S'07) received the B.S. degree from Seoul National University in 2003 and the M.S. degree from Georgia Institute of Technology in 2008. He has been working toward his Ph.D. degree in Georgia Tech Analog, Power, and Energy IC Lab since spring 2007. From 2003 to 2006, he worked as a research engineer in Hantel Inc., Kyunggi, Korea and developed MP3 players. From August to December 2010, he worked as a design intern at Linear Technology Corporation, Milpitas, CA, and implemented a switching power converter IC. His research interests include piezoelectric energy harvesting circuits, switching-mode power ICs, and ultra-low-power analog IC design. He won the 2nd place in the 2009 Science Applications International Corporation-Georgia Tech student paper competition.

Gabriel A. Rincón-Mora (S'91-M'97-SM'01-F'11) received his B.S., M.S., and Ph.D. in electrical engineering, is an IET Fellow, and worked for Texas Instruments in '94-'03, was Adjunct Professor at Georgia Tech in '99-'01, and is a full-time faculty member at Georgia Tech since '01. His scholarly products include 8 books, 1 book chapter, over 125 scientific publications, 37 patents, over 26 commercial chip designs, and over 60 international speaking engagements. He received the "National Hispanic in Technology Award," "Charles E. Perry Visionary Award," a "Commendation Certificate" from the Lieutenant Governor of California, IEEE CASS Service Award, and Robins Air Force Base's "Orgullo Hispano" and "Hispanic Heritage" awards. He was inducted into Georgia Tech's "Council of Outstanding Young Engineering Alumni," elected IEEE CASS Distinguished Lecturer for '09-'10, and featured on the cover of Hispanic Business magazine as one of "The 100 Most Influential Hispanics." He is Associate Editor for IEEE's TCAS II; Editorial Board Member for JOLPE; Chairman of Atlanta's IEEE SSCS-CASS Chapter; Technical Committee Member for IEEE's CASS ASP and PECAS; Steering Committee Member for IEEE's MWSCAS; was General Chair for SRC's Energy and Power ICs Workshop in '09; Circuit Design Vice Chair for IEEE's '08 ICCDCS; Technical Program Chair for IEEE's '07 MWSCAS-NEWCAS; and Technical Program Co-Chair for IEEE's '06 MWSCAS.

Erick O. Torres was born and raised in San Juan, Puerto Rico. He received the B.S. degree from the University of Central Florida in 2003 and the M.S. and Ph.D. degrees from the Georgia Institute of Technology in 2006 and 2010, respectively, all in electrical engineering. While a Ph.D. student in the Georgia Tech Analog, Power, and Energy IC Design Research Lab, he researched, designed, and developed electrostatic harvester ICs. He has been awarded several fellowships, including the Goizueta Foundation Fellowship (2003–2007), the Georgia Tech President's Fellowship (2003–2008), and the Texas Instruments' Analog Fellowship (2005–2009). Currently, he is an analog IC designer with the Mixed-Signal Automotive group in Texas Instruments, Inc., Dallas, TX.